IEEE Access
Multidisciplinary ⋮ Rapid Review ⋮ Open Access Journal

Received October 7, 2021, accepted October 17, 2021, date of publication October 27, 2021, date of current version November 9, 2021.

Digital Object Identifier 10.1109/ACCESS.2021.3123365

Discrete-Time Analysis and Synthesis of Disturbance Observer-Based Robust Force Control Systems

EMRE SARIYILDIZ[1], (Senior Member, IEEE), SATOSHI HANGAI[2], (Member, IEEE), TARIK UZUNOVIC[3], (Senior Member, IEEE), AND TAKAHIRO NOZAKI[2], (Member, IEEE)

[1]Faculty of Engineering and Information Sciences, School of Mechanical, Materials, Mechatronic and Biomedical Engineering, University of Wollongong, Wollongong, NSW 2522, Australia
[2]Department of System Design Engineering, Faculty of Science and Technology, Keio University, Yokohama 223-8522, Japan
[3]Department of Automatic Control and Electronics, Faculty of Electrical Engineering, University of Sarajevo, 71000 Sarajevo, Bosnia and Herzegovina

Corresponding author: Emre Sariyildiz (emre@uow.edu.au)

This work was supported in part by JSPS KAKENHI Grant Number JP19KK0367, and in part by the Ministry for Science, Higher Education and Youth of Canton Sarajevo.

ABSTRACT This paper analyses Disturbance Observer- (DOb-) based robust force control systems in the discrete-time domain. The robust force controller is implemented using velocity and acceleration measurements. A DOb is employed in an inner-loop to achieve robustness, and another DOb, viz. Reaction Force Observer (RFOb), is employed in an outer-loop to estimate interaction forces and improve the performance of force control. First, the inner-loop is analysed. It is shown that the DOb works as a phase-lead/lag compensator tuned by the nominal design parameters in the inner-loop. The phase margin of the inner-loop controller and the bandwidth of the velocity-based (i.e., conventional) DOb are constrained not only by noise-sensitivity but also by the waterbed effect. This explains why we observe unstable responses as the bandwidth of the conventional DOb increases in practice. To eliminate the design constraint due to the waterbed effect, this paper proposes an acceleration-based DOb. Then, the robust force controller is analysed. It is shown that the design parameters of the RFOb have a notable effect on the stability of the robust force control system. For example, the robust force controller has a non-minimum phase zero (zeros) when the RFOb is not properly tuned. This may cause severe stability and performance problems when conducting force control applications. By using the stability and robustness analyses, this paper proposes new design tools which enable one to synthesize a high-performance robust force control system. Simulations and experiments are presented to validate the proposed analysis and synthesis methods.

INDEX TERMS Discrete-time control, disturbance observer, force control, robustness, reaction force observer, robust stability and performance.

I. INTRODUCTION

With the significant paradigm shifts in the 21st century, physical robot-environment interaction has become a compelling demand in various engineering applications [1]–[3]. For example, while collaborative robots that can work in an open factory setting have been established to meet the requirements of the 4th industrial revolution, wearable robots that can interact with human beings have been developed to help improve the quality of life in ageing societies [2], [3]. It is a well-known fact that precise positioning is insufficient and high-performance force control is crucial to safely interact with an unknown and dynamic environment [3]–[5]. Despite many attempts, the stability and low-performance of force control systems that interact with unstructured environments are still challenging problems in the fields of motion control and robotics [5].

One of the main challenges in physical interaction control is that internal disturbances, such as friction at joints, and varying environmental dynamics may have a notable impact on the stability and performance of force control systems [5], [6]. To tackle this problem, various adaptive and robust force controllers have been proposed in the literature [5]–[9]. Among them, the DOb-based robust force

The associate editor coordinating the review of this manuscript and approving it for publication was Shihong Ding.

controller has been widely adopted by researchers due to its simplicity and efficacy [10]–[12]. It has been applied to various engineering applications, and its superiorities over other force control methods have been reported in many different studies. For example, real-haptic sensation can be obtained by using the DOb-based robust force controller [13], [14], contact forces can be explicitly estimated without changing the compliance of the motion control system [5], and the stability and performance of physical interaction control can be notably improved by estimating contact forces within a large bandwidth via the RFOb [15]. In addition, force-sensorless contact force estimation helps reduce the size and mechanical complexity of robotic systems as well as the cost of engineering projects [12]. Compared to a force sensor, the main drawback of this sensorless force control method is that internal disturbances should be identified to accurately estimate contact forces via the RFOb [10].

To implement the robust force controller, the nominal design parameters (i.e., nominal mass and force coefficient) and the bandwidths of the DOb and RFOb should be tuned. In general, actual mass and force coefficient values are used in the observer synthesis [8], [12], [16]. By considering the noise-sensitivity of the controller, the bandwidths of the DOb and RFOb are set as high-as possible to improve the performance of force estimation within a large frequency range [12]. Several studies have been conducted to enhance the bandwidth of the DOb. For example, Katsura *et al.* [17] proposed a Position-Acceleration Integrated Disturbance Observer, viz. PAIDO, to widen the bandwidth of force estimation. Mitsantisuk *et al.* [18] and Phuong *et al.* [19] used Kalman filter to suppress noise and increase the bandwidth of the DOb.

There are two main drawbacks of the conventional design approach which suggests that the nominal parameters of the DOb-based robust motion controller should be tuned using the exact plant model: i) The exact plant model (e.g., the inertia matrix of a robotic system) may not be identified in practice [20], and ii) The nominal design parameters can be used to adjust the stability and performance, thus providing extra flexibility in controller synthesis [5], [8]. Few studies showed that not only the bandwidth but also the nominal design parameters of the DOb and RFOb may significantly change the stability and performance of the robust force controller. For example, Murakami *et al.* and Kobayashi *et al.* showed that the stability of the robust force controller can be adjusted by tuning the nominal mass and force coefficient in the DOb synthesis in [16], [20]. Sariyildiz and Ohnishi [8] showed that the design parameters of the RFOb can also be used to adjust the stability of the robust force controller.

Although the DOb-based robust force controllers are always implemented using digital controllers, they are generally analysed in the continuous-time domain due to simplicity [8], [12], [19]– [21]. Continuous-time analysis methods, however, fall-short in explaining the robust stability and performance of the DOb-based motion controllers implemented by computers or microcontrollers [22]–[24]. For example, continuous-time analysis methods cannot explain why the stability of the digital robust motion controller deteriorates as the bandwidth of the conventional DOb increases [23], [24]. To improve the performance of the DOb-based robust digital motion control systems, new analysis and synthesis methods have been proposed in [22]–[30]. Nevertheless, the stability and robustness of the DOb-based digital force control systems have yet to be analysed in the discrete-time domain. Therefore, although the robust force controller has been applied to various engineering systems in the last three decades, the bandwidth and nominal design parameters of the DOb and RFOb are still tuned manually, by trial and error in practice.

To this end, this paper analyses the stability and robustness of the DOb-based force control systems in the discrete-time domain. By employing the discrete Bode Integral Theorem, it is shown that the bandwidth of the conventional DOb is limited not only by the noise-sensitivity of velocity measurement systems but also by the waterbed effect. Therefore, the robust stability and performance of the digital motion controller deteriorate as the bandwidth of the conventional DOb increases in practice. When acceleration measurement is used in the DOb synthesis, the robust motion controller is not subject to the waterbed effect. In other words, the bandwidth of the acceleration-based DOb is limited by only the noise-sensitivity of acceleration measurement systems. This paper also shows that the mass and force coefficient terms of the DOb and RFOb have a notable effect on the stability and performance of the robust force controller. For example, while increasing the nominal mass term of the DOb improves phase-lead effect in the inner-loop, using higher values of the identified mass term in the RFOb synthesis significantly deteriorates the stability of the robust force controller due to a non-minimum phase zero(s). To improve the stability of the robust force controller, lower (higher) values of the identified mass (force coefficient) term should be employed in the RFOb synthesis. This paper, for the first time, clearly explains the design constraints of the DOb-based digital robust force control systems. Within this context, the chief contributions of this paper are as follows.

i) By employing the generalised Bode Integral Theorem in the discrete-time domain, this paper, for the first time, derives the design constraints of the DOb-based digital robust force controllers. This allows one to explain the unexpected stability and performance problems encountered in practice.
ii) To eliminate the design constraints due the waterbed effect, this paper, for the first time, proposes an acceleration-based robust force controller. This allows one to improve the stability and performance of the robust force control system by widening the frequency range of disturbance and contact force estimation via the DOb and RFOb, respectively.
iii) Compared to conventional design approach, this paper, for the first time, shows that high-performance force control applications can be performed by tuning the nominal design parameters of the DOb and RFOb.

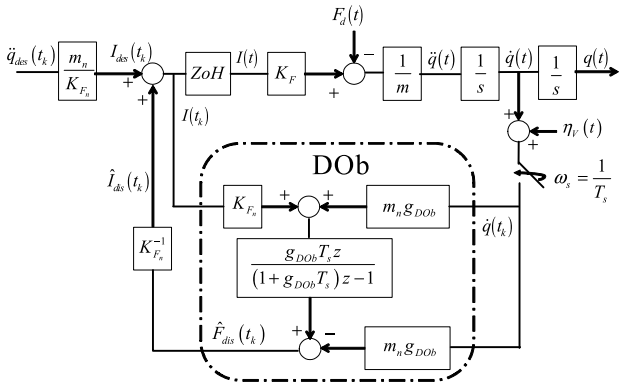

FIGURE 1. Block diagram of the conventional DOb that is implemented by estimating the velocity state of a servo system.

This statement is proven by a theoretical explanation and experimental verifications.

The rest of the paper is organised as follows. Section II analyses the stability and robustness of the DOb by considering velocity and acceleration measurements in the discrete-time domain. The design constraints of the DOb are analytically derived. Section III analyses the robust force control systems. It is shown that the stability and performance of the robust force controller can be adjusted by tuning the design parameters of the DOb and RFOb. Section IV presents simulations and experiments to verify the proposed analysis and synthesis methods. The paper ends with conclusion given in Section V.

II. DISTURBANCE OBSERVER

A. CONVENTIONAL DISTURBANCE OBSERVER

Fig. 1 illustrates the block diagram of the conventional DOb that is implemented using velocity measurement. The following apply in this figure:

m, m_n	uncertain and nominal masses;
K_F, K_{F_n}	uncertain and nominal force coefficients;
$q,\ \dot{q}, \ddot{q}$	position, velocity, and acceleration;
t, t_k	time in the continuous and discrete domains;
T_s	sampling time;
ω_s	sampling frequency;
g_{DOb}	bandwidth of the DOb;
I	thrust current of the motor;
F_d	external disturbance force;
η_V	noise in velocity measurement;
ZoH	Zero-order Hold;
F_{dis}	internal and external disturbance force;
I_{dis}	internal and external disturbance current;
$\hat{\bullet}$	estimation of $\bullet$;
$\bullet_{des}$	desired $\bullet$;
s	complex Laplace variable;
$z = e^{sT_s}$	complex variable.

The conventional DOb estimates the internal and external disturbances (e.g., friction, parameter variations, and load) of a servo system by using the applied motor current, velocity measurement, nominal plant model, and a low-pass filter as illustrated in Fig. 1. The robustness of the motion controller is intuitively achieved by feeding back the estimated disturbances via an inner-loop control structure [12]. The discrete transfer function of the inner-loop from the desired acceleration input to the resulting motor velocity can be directly derived from Fig. 1 as follows:

$$\dot{q}\,(z) = \alpha P_V\,(z)\,I\,(z)\,\ddot{q}_{des}\,(z) \tag{1}$$

where $\alpha = (m_n K_F)/\left(m K_{F_n}\right)$; $P_V\,(z) = \frac{(1+g_{DOb}T_s)z-1}{z-(1-\alpha g_{DOb}T_s)}$ is a phase-lead/lag compensator and $I\,(z) = \frac{T_s}{z-1}$ is an integrator.

Equation (1) shows that the phase-lead/lag compensator $P_V\,(z)$ is obtained in the inner-loop when the conventional DOb is used in the robust motion controller synthesis. While $P_V\,(z)$ is a phase-lead compensator when the design parameters hold $\alpha > (1 + g_{DOb}T_s)^{-1}$, tuning the DOb by using $\alpha < (1 + g_{DOb}T_s)^{-1}$ results in the phase-lag compensator $P_V\,(z)$ in the inner-loop. The phase-margin of the inner-loop improves as α is increased.

Equation (1) also shows that the robust motion controller is unstable when $\alpha g_{DOb} > 2\omega_s$ and exhibits oscillatory response when $\omega_s < \alpha g_{DOb} < 2\omega_s$. To achieve good stability by placing the discrete pole of $P_V\,(z)$ between 0 and 1, the design parameters of the DOb should be tuned using $\alpha g_{DOb} < \omega_s$. In other words, the model-plant mismatch and the bandwidth of the conventional DOb have upper bounds due to the stability constraint. Without degrading the stability, the phase margin and robustness of the motion control system can be improved (i.e., higher values of α and g_{DOb} can be used in the design of the DOb) by increasing the sampling frequency ω_s. However, this generally leads to cost increase in motion control systems.

The sensitivity and complementary sensitivity functions of the robust motion control system can be similarly derived from Fig. 1 as follows:

$$S_V\,(z) = \frac{z-1}{z-(1-\alpha g_{DOb}T_s)} \tag{2}$$

$$T_V\,(z) = \frac{\alpha g_{DOb}T_s}{z-(1-\alpha g_{DOb}T_s)} \tag{3}$$

where $S_V\,(z)$ and $T_V\,(z)$ are the sensitivity and complementary sensitivity functions of the conventional DOb in the discrete-time domain, respectively.

Equation (2) shows that the magnitude of the sensitivity function $|S_V\,(z)|$ decreases at low frequencies (i.e., the robustness against disturbances improves) as higher values of α and g_{DOb} are used in the DOb synthesis. This, however, makes the robust motion controller more sensitive to the noise in velocity measurement because the complementary sensitivity function is suppressed less at high frequencies as shown in (3). The trade-off between the robustness against disturbances and the noise-sensitivity of the conventional DOb is well-known in the literature [12].

In addition, improving the robustness against disturbances at low frequencies by increasing the design parameters α and g_{DOb} may result in a high-sensitivity peak at middle/high

frequencies in the conventional DOb-based robust motion control systems. This phenomenon is called waterbed effect in the literature and can be analysed by employing the Bode's integral equation [31], [32]. If the Bode Integral Theorem is applied to the motion control system shown in Fig. 1 in the discrete-time domain, then the following equation is obtained.

$$\int_{-\pi}^{\pi} \ln |S_V(z)|\, d\omega T_s = -2\pi \ln \left| 1 + \lim_{z\to\infty} \frac{\alpha g_{DOb} T_s}{z-1} \right| = 0 \qquad (4)$$

where ω represents frequency, $z = e^{j\omega T_s}$ and $j^2 = -1$ [32].

Equation (4) shows that as $|S_V(z)|$ is decreased at low frequencies by increasing the design parameters of α and/or g_{DOb}, the peak of the sensitivity function becomes larger at higher frequencies to hold the Bode's integral equation. The robust motion controller may suffer from the waterbed effect if the nominal plant model and the bandwidth of the DOb are not properly tuned. This explains why we observe unstable responses as the bandwidth of the conventional DOb is increased in practice [17], [23], [24]. The waterbed effect brings another constraint (called robustness constraint in this paper) on the design parameters of the conventional DOb.

It is noted that the robustness constraint on the design parameters of the conventional DOb cannot be derived by conducting analysis in the continuous-time domain. To prove this statement, let us again use the Bode's integral equation. If the Bode Integral Theorem is applied to the conventional DOb-based robust motion controller in the continuous-time domain as recommended in [8], then the following equation is obtained.

$$\int_{0}^{\infty} \log\left(|S_V(s)|\right) d\omega = -\frac{\pi}{2} \alpha g_{DOb} \qquad (5)$$

where $S_V(s) = \frac{s}{s+\alpha g_{DOb}}$ is the sensitivity function of the conventional DOb in the continuous-time domain, and $s = j\omega$ is the complex Laplace variable [8].

Since the right side of (5) gets smaller as the robustness against disturbances is improved by increasing α and/or g_{DOb}, the Bode's integral equation can hold without exhibiting a high-sensitivity peak. In other words, the continuous-time analysis shows that the conventional DOb-based robust motion controller is not subject to the waterbed effect and good robust stability and performance can be achieved for all values of α and g_{DOb}. In fact, the stability of the DOb implemented by digital controllers deteriorates as α and g_{DOb} are increased [23], [24]. Continuous time analysis methods, therefore, fall-short in explaining the dynamic behaviours of the conventional DOb-based digital robust motion control systems in practice.

The design constraints on the bandwidth of the DOb and plant-model mismatch become more severe when the plant includes time-delay [33]. This, for example, occurs when the DOb is applied to teleoperated robotic systems [34]. For the sake of brevity, time-delay problem is not considered in this paper. Reader is referred to [33] for the design constraints of the DOb-based robust control systems with time-delay.

B. ACCELERATION-BASED DISTURBANCE OBSERVER

Let us now consider a DOb that is implemented by estimating the acceleration state of a servo system rather than velocity. The block diagram of the acceleration-based DOb is illustrated in Fig. 2. In this figure, η_A represents the noise in acceleration measurement, and the other parameters are same as defined earlier.

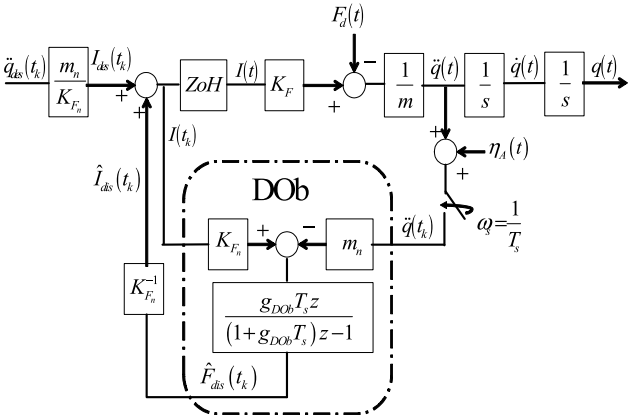

FIGURE 2. Block diagram of the DOb that is implemented by estimating the acceleration state of a servo system.

The discrete transfer function from the desired acceleration input to the resulting motor acceleration can be similarly derived from Fig. 2 as follows:

$$\ddot{q}(z) = \alpha P_A(z)\, \ddot{q}_{des}(z) \qquad (6)$$

where $P_A(z) = \frac{(1+g_{DOb}T_s)z-1}{(1+\alpha g_{DOb}T_s)z-1}$ is a phase-lead/lag compensator when acceleration measurement is used in the DOb synthesis.

Equation (6) shows that $P_A(z)$ is a phase-lead (phase-lag) compensator when the design parameters of the acceleration-based DOb is tuned by using $\alpha > 1$ ($\alpha < 1$). The phase margin of the system can be similarly improved by increasing α. The acceleration-based DOb, however, is stable for all values of α and g_{DOb}. Therefore, there is no stability constraint on the design parameters of the DOb when it is synthesised using acceleration measurement.

The Bode integral equation of the DOb-based robust motion control system shown in Fig. 2 is as follows:

$$\int_{-\pi}^{\pi} \ln |S_A(z)|\, d\omega T_s = -2\pi \ln \left| 1 + \lim_{z\to\infty} \frac{\alpha g_{DOb} T_s z}{z-1} \right| = -2\pi \ln |1 + \alpha g_{DOb} T_s| \qquad (7)$$

where $S_A(z) = \frac{z-1}{(1+\alpha g_{DOb}T_s)z-1}$ is the sensitivity function of the acceleration-based DOb [31].

Similarly, the magnitude of the sensitivity function $|S_A(z)|$ decreases (i.e., disturbance attenuation improves) at low

frequencies as α and/or g_{DOb} are increased. This, however, does not result in a high sensitivity peak in the acceleration-based DOb. Since the right side of (7) gets smaller with higher values of α and/or g_{DOb}, the Bode's integral equation can hold without exhibiting a high sensitivity peak. Therefore, the robust motion controller is not subject to the waterbed effect when acceleration measurement is used in the DOb synthesis.

Compared to the conventional DOb, the design parameters of the acceleration-based DOb are not influenced by the stability and robustness constraints. Nevertheless, neither α nor g_{DOb} can be freely tuned in practice. Since the complementary sensitivity function given in (8) is suppressed less as α and/or g_{DOb} are increased, the robust motion controller becomes more sensitive to the noise in acceleration measurement. Thus, the trade-off between the robustness against disturbances and the noise-sensitivity of the robust motion controller determines the design constraints of the acceleration-based DOb.

$$T_A(z) = \frac{\alpha g_{DOb} T_s z}{(1 + \alpha g_{DOb} T_s) z - 1} \tag{8}$$

where $T_A(z)$ is the complementary sensitivity function of the acceleration-based DOb

III. DISTURBANCE OBSERVER-BASED ROBUST FORCE CONTROL

A. ACCELERATION-BASED ROBUST FORCE CONTROLLER

Fig. 3 illustrates the DOb-based robust force control system which is implemented using acceleration measurement. The following apply in this figure.

m_i	identified motor mass;
K_{F_i}	identified force coefficient;
g_{RFOb}	bandwidth of the RFOb;
C_F	proportional gain of the force controller;
F_{ref}	force reference;
F_{ext}	contact force;
D_{env}	damping of the environment;
K_{env}	stiffness of the environment;
$F_i(t_k)$	identified disturbance force;
$e_F(t_k)$	force error, i.e., $F_{ref}(t_k) - \hat{F}_{ext}(t_k)$.

and the other parameters are same as defined earlier.

The robust force controller is synthesised by employing the DOb and RFOb in the inner- and outer-loop, respectively. The DOb improves the robustness of the force control system by suppressing disturbances, such as friction and load, in the inner-loop. The contact force is estimated by using the RFOb, which is simply synthesised by subtracting the identified disturbances from a DOb, in the outer-loop. Since the RFOb can explicitly estimate contact forces within a large frequency range, it provides better stability and performance than force sensors in physical interaction control [8], [15]. Moreover, force-sensorless contact force estimation has several advantages, such as reducing cost, in engineering applications. The accuracy of contact force estimation is, however, directly

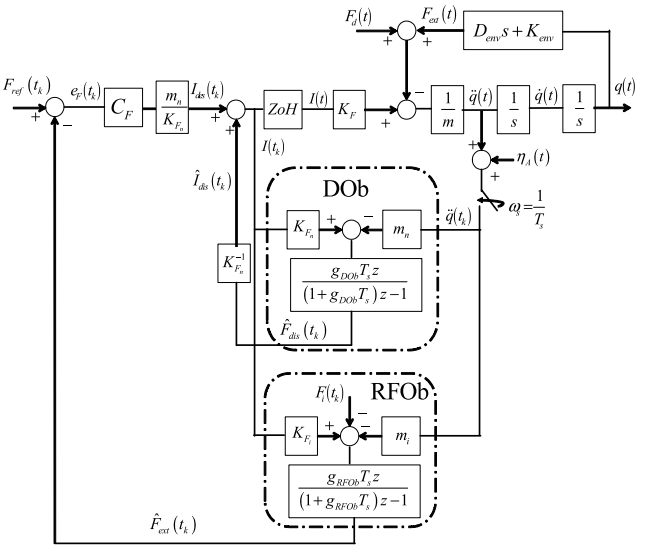

FIGURE 3. Block diagram of the DOb-based robust force control system that is implemented using acceleration measurement.

influenced by the identification of disturbances. The reader is referred to [5], [8], [35] for further details on the robust force control systems implemented by the RFOb and force sensors.

The open-loop transfer function of the robust force control system (i.e., the transfer function between $e_F(t_k)$ and $\hat{F}_{ext}(t_k)$) can be derived from Fig. 3 as follows:

$$\mathrm{L_A}(z) = \hat{C}_F \frac{T_s z}{z-1} \Phi_{\mathrm{L}}(z)\, \Phi_{\mathrm{A}}(z) \tag{9}$$

where $\hat{C}_F = C_F m_i g_{RFOb} \beta$ is the open-loop force control gain in which $\beta = (m_n K_{F_i})/(m_i K_{F_n})$; $\Phi_{\mathrm{L}}(z) = \frac{(1+g_{DOb}T_s)z-1}{(1+g_{RFOb}T_s)z-1}$ is a phase-lead/lag compensator; and (10), as shown at the bottom of the next page, where $\delta = \alpha/\beta = (m_i K_F)/(m K_{F_i})$, $\omega_0 = \sqrt{K_{env}/m}$, $\xi = D_{env}/2\omega_0 m$, $\omega_n = \omega_0\sqrt{1-\xi^2}$ and $\rho = \mathrm{e}^{-\xi\omega_0 T_s}\left(\cos(\omega_n T_s) + \left(\xi/\sqrt{1-\xi^2}\right)\sin(\omega_n T_s)\right)$.

Equation (9) shows that there is an integrator in the open-loop transfer function of the robust force control system. Therefore, the robust force controller can remove the steady-state error in force regulation. This equation also shows that the phase-lead/lag compensator $\Phi_{\mathrm{L}}(z)$ can be used to adjust the stability and performance of the robust force controller. $\Phi_{\mathrm{L}}(z)$ is a phase-lead (phase-lag) compensator when the robust force controller is synthesised by using $g_{DOb} < g_{RFOb}$ ($g_{DOb} > g_{RFOb}$), and the phase margin of the robust force control system improves as g_{RFOb} is increased.

In addition to the integrator and phase-lead/lag compensator, the open-loop transfer function of the robust force control system includes the second-order transfer function $\Phi_{\mathrm{A}}(z)$ given in (10). The dynamics of $\Phi_{\mathrm{A}}(z)$ changes not only by the design parameters of the robust force controller but also by the impedance of environment. Let us consider the transfer function $\Phi_{\mathrm{A}}(z)$ in detail because it has a notable

effect on the stability and performance of the robust force control system.

Equation (10) shows that the poles of $\Phi_{\mathrm{A}}(z)$ move from $\mathrm{e}^{-\xi\omega_0 T_s + j\omega_n T_s}$ to 0 and ρ as α and/or g_{DOb} are increased. The imaginary parts of the poles become larger as the stiffness (damping) of the environment increases (decreases). To suppress the oscillatory poles of $\Phi_{\mathrm{A}}(z)$ when the servo system physically interacts with a stiff environment, we need to use higher values of α and/or g_{DOb} in the DOb synthesis and increase the sampling frequency. However, the design parameters of the robust force control system and sampling frequency cannot be freely tuned due to practical constraints such as the noise of accelerometers and the computing power of processors.

Equation (10) also shows that the transfer function $\Phi_{\mathrm{A}}(z)$ has a zero between -1 and 1 and the relative degree of the open-loop transfer function is one when the exact values of mass and force coefficient are used in the RFOb synthesis (i.e., $\delta = 1$, or $m_i = m$ and $K_{F_i} = K_F$). As the force control gain C_F increases, the stability of the robust force control system deteriorates because the closed-loop pole of the force controller moves towards infinity. The stability constraint on the force control gain limits the bandwidth of the robust force control system. When the exact mass and force coefficient values are not used in the RFOb synthesis (i.e., $\delta \neq 1$), the transfer function $\Phi_{\mathrm{A}}(z)$ has two zeros and the relative degree of the open-loop transfer function is zero. Each closed-loop pole of the robust force control system converges to a finite value (i.e., to an open-loop zero) as the force control gain C_F is increased. However, the stability of the robust force controller significantly changes by the design parameter δ. When $\delta > 1$, the open-loop transfer function has a zero outside the unit circle. The non-minimum phase zero degrades the stability of the robust force controller and results in new design constraints such as a strict limitation in force control bandwidth. To achieve minimum phase zeros, the robust force controller should be synthesised by using $\delta < 1$ (i.e., $m_i < m$ and/or $K_{F_i} > K_F$) and

$$\delta < \frac{\mathrm{e}^{-2\xi\omega_0 T_s} + 2\mathrm{e}^{-\xi\omega_0 T_s}\cos(\omega_n T_s) + 1}{2(1+\rho)} \tag{11}$$

As shown in (9) and (11), the dynamics of environment has a notable effect on the stability and performance of the robust force controller. To conduct high-performance force control applications in practice, the force control gain should be tuned by considering environmental impedance as shown in Fig. 7 in Section IV [5].

B. CONVENTIONAL ROBUST FORCE CONTROLLER

The robust force controller can be similarly synthesised by using the conventional DOb as shown in Fig. 4.

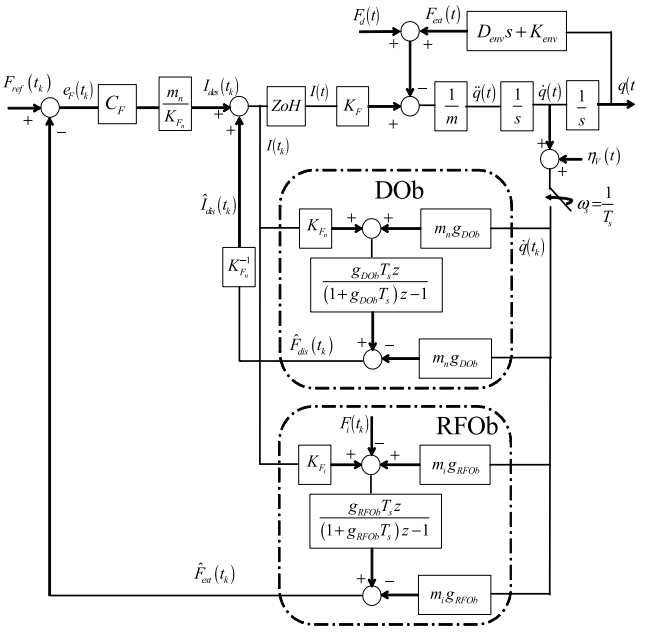

FIGURE 4. Block diagram of the conventional DOb-based robust force control system that is implemented using velocity measurement.

The open-loop transfer function of the conventional DOb-based robust force control system can be derived from this figure as follows:

$$\mathrm{L_V}(z) = \hat{C}_F \beta \frac{T_s z}{z-1} \Phi_{\mathrm{L}}(z)\, \Phi_{\mathrm{V}}(z) \tag{12}$$

where $\Phi_{\mathrm{V}}(z) = \Phi_{\mathrm{V_n}}(z) \big/ \Phi_{\mathrm{V_d}}(z)$ in which

$$\begin{aligned}\Phi_{\mathrm{V_n}}(z) &= z^3 - \left(2\mathrm{e}^{-\xi\omega_0 T_s}\cos(\omega_n T_s) + \delta \mathrm{e}^{-\xi\omega_0 T_s}\mathrm{sinc}(\omega_n T_s)\right) z^2 \\ &\quad + \left(\mathrm{e}^{-2\xi\omega_0 T_s} + 2\delta \mathrm{e}^{-\xi\omega_0 T_s}\mathrm{sinc}(\omega_n T_s)\right) \\ &\quad \times z - \delta \mathrm{e}^{-\xi\omega_0 T_s}\mathrm{sinc}(\omega_n T_s)\end{aligned} \tag{13}$$

$$\begin{aligned}\Phi_{\mathrm{V_d}}(z) &= z^3 - \left(2\mathrm{e}^{-\xi\omega_0 T_s}\cos(\omega_n T_s)\right. \\ &\quad \left. -\alpha g_{DOb} T_s \mathrm{e}^{-\xi\omega_0 T_s}\mathrm{sinc}(\omega_n T_s)\right) z^2 \\ &\quad + \left(\mathrm{e}^{-2\xi\omega_0 T_s} - \alpha g_{DOb} T_s \mathrm{e}^{-\xi\omega_0 T_s}\mathrm{sinc}(\omega_n T_s)\right) z\end{aligned} \tag{14}$$

where $\mathrm{sinc}(\omega_n T_s) = \sin(\omega_n T_s)/\omega_n T_s$.

Equation (12) shows that the open-loop transfer function $\mathrm{L_V}(z)$ includes the same open-loop force control gain, integrator, and the first order phase-lead/lag compensator of $\mathrm{L_A}(z)$ given in (9). Therefore, similarly, the steady-state error can be removed in force regulation and the phase margin of the force control system can be adjusted by tuning the

$$\Phi_{\mathrm{A}}(z) = \frac{(1-\delta) z^2 - \left(2\mathrm{e}^{-\xi\omega_0 T_s}\cos(\omega_n T_s) - \delta(1+\rho)\right) z + \mathrm{e}^{-2\xi\omega_0 T_s} - \delta\rho}{(1+\alpha g_{DOb} T_s) z^2 - \left(2\mathrm{e}^{-\xi\omega_0 T_s}\cos(\omega_n T_s) + \alpha g_{DOb} T_s \rho\right) z + \mathrm{e}^{-2\xi\omega_0 T_s}} \tag{10}$$

bandwidths of the DOb and RFOb. However, the dynamics of the robust force control systems illustrated in Fig. 3 and Fig. 4 are different due to the transfer functions of $\Phi_A(z)$ and $\Phi_V(z)$.

As $\alpha g_{DOb} T_s$ increases, two poles of $\Phi_V(z)$ move from $e^{-\xi\omega_0 T_s \pm j\omega_n T_s}$ to 1 and ∞ while its third pole stays at zero. To achieve stable poles for $L_V(z)$, smaller sampling time is needed for higher values of α and g_{DOb}. This is consistent with the inner-loop design constraint $\alpha g_{DOb} < \omega_s$ derived in Section II. In addition, using smaller sampling time yields less oscillatory poles for the transfer function $\Phi_V(z)$ when the motion control system physically interacts with a stiff environment.

The zeros of $\Phi_V(z)$ move from 0 and $e^{-\xi\omega_0 T_s \pm j\omega_n T_s}$ to 1, 1 and ∞ as $\delta e^{-\xi\omega_0 T_s} \mathrm{sinc}(\omega_n T_s)$ increases. Similarly, the conventional DOb-based robust force control system has non-minimum phase zeros if the design parameters are not properly tuned. For example, increasing δ results in a non-minimum phase zero. To improve the stability of the robust force control system, δ and the sampling time T_s should be decreased, particularly when contacting with a stiff environment.

It is noted that although $\Phi_V(z)$ is different from $\Phi_A(z)$, the open-loop transfer functions $L_V(z)$ and $L_A(z)$ have very similar dynamic characteristics. For example, both of the robust force control systems have a non-minimum phase zero(s) for high values of the control parameter δ, and the open-loop transfer functions have more oscillatory poles as the sampling time and environmental stiffness increase. However, the design constraints of the conventional DOb-based robust force control system are stricter than that of the acceleration-based robust force control system.

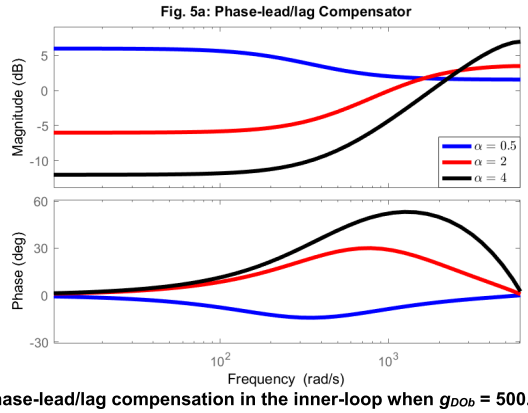

a) Phase-lead/lag compensation in the inner-loop when g_{DOb} = 500.

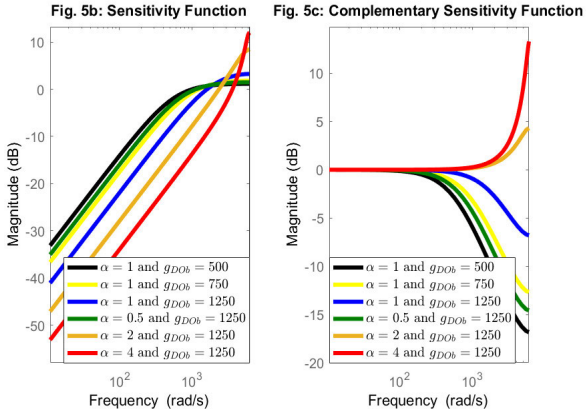

b) Sensitivity Function; c) Complementary Sensitivity Function.

FIGURE 5. Frequency responses of $P_V(z)$, $S_V(z)$, and $T_V(z)$ when $m = 0.025$, $K_{Fn} = K_F = 0.675$, and $T_s = 0.5 \times 10^{-3}$.

IV. SIMULATIONS AND EXPERIMENTS

A. SIMULATIONS

Let us first consider the robust stability and performance of the conventional and acceleration-based DObs. Fig. 5 illustrates the frequency responses of the phase-lead/lag compensator and the sensitivity and complementary sensitivity functions of the conventional DOb-based robust motion control system illustrated in Fig. 1. Fig. 5a shows that the phase-margin of the inner-loop can be adjusted by tuning the nominal design parameters. The phase margin of the system improves by simply using higher values of α in the DOb synthesis. Figs. 5b and 5c illustrate the sensitivity and complementary sensitivity functions. As either α or g_{DOb} increases, the sensitivity function becomes smaller and the robustness against disturbances improves at low frequencies (see Fig. 5b). However, the noise of velocity measurement is suppressed less and the peaks of the sensitivity and complementary sensitivity functions dramatically increase for the high values of α and g_{DOb} (see Fig. 5c). The sensitivity peaks not only excite the disturbances at high frequencies, such as noise, but also degrade the robust stability of the motion control system. For example, as shown in Section II, the conventional DOb-based robust motion controller is unstable when $\alpha g_{DOb} > 2\omega_s$. Therefore, the plant-model mismatch and the bandwidth of the conventional DOb are limited by the waterbed effect in addition to the noise-sensitivity of velocity measurement systems.

Fig. 6 illustrates the frequency responses of the phase-lead/lag compensator and the sensitivity and complementary sensitivity functions of the acceleration-based DOb illustrated in Fig. 2. The phase margin of the robust motion controller can be similarly improved by increasing α in the DOb synthesis (see Fig. 6a). Fig. 6b and 6c show that the waterbed effect is not observed and good robust stability and performance can be achieved for all values of α and g_{DOb} when the robust motion controller is implemented using the acceleration-based DOb. However, increasing the design parameters α and/or g_{DOb} still degrades the noise-sensitivity of the robust motion controller because the complementary sensitivity function is suppressed less at high frequencies (see Fig. 6c). The robustness of the acceleration-based DOb is limited by only the noise-sensitivity of acceleration measurement systems in practice.

Let us now consider the stability of the DOb-based robust force control system. The root-loci of the conventional and acceleration-based robust force controllers are illustrated for

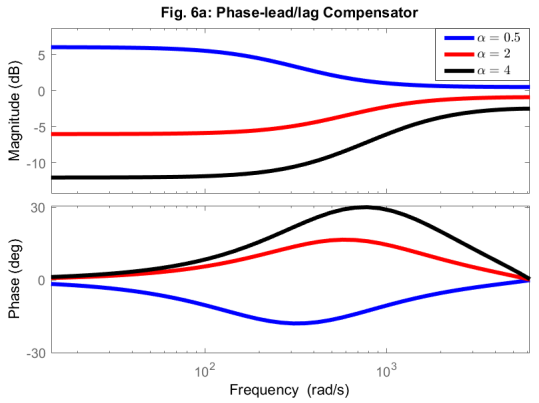

a) Phase-lead/lag compensation in the inner-loop when $g_{DOb} = 500$.

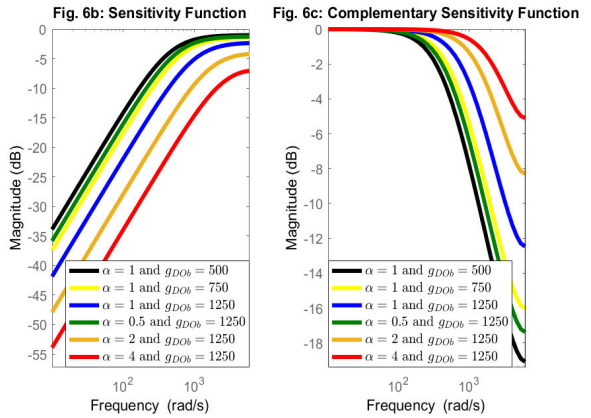

b) Sensitivity Function; c) Complementary Sensitivity Function.

FIGURE 6. Frequency responses of $P_A(z)$, $S_A(z)$, and $T_A(z)$ when $m = 0.025$, $K_{Fn} = K_F = 0.675$, and $T_s = 0.5 \times 10^{-3}$.

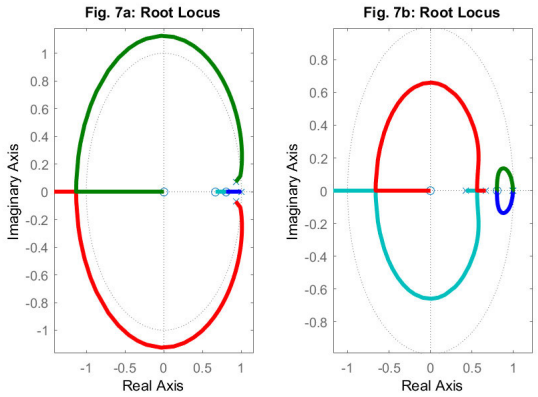

a) α = 0.2, K_{env} = 275, g_{DOb} = 500, g_{RFOb} = 250 and T_s = 1x10^{-3}; b) α = 5, K_{env} = 275, g_{DOb} = 250, g_{RFOb} = 500 and T_s = 1x10^{-3}.

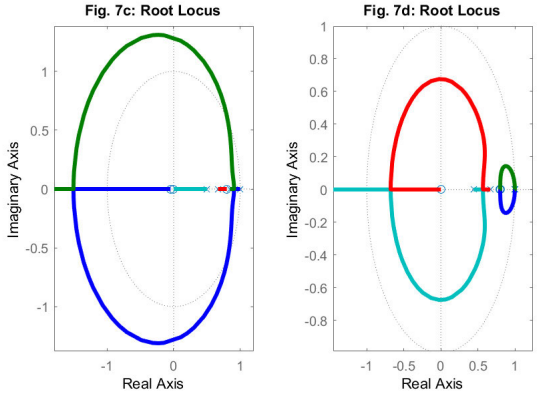

c) α = 5, K_{env} = 2750, g_{DOb} = 250, g_{RFOb} = 500 and T_s = 1x10^{-3}; d) α = 5, K_{env} = 2750, g_{DOb} = 2500, g_{RFOb} = 5000 and T_s = 0.1x10^{-3}.

FIGURE 7. Root-loci of the acceleration-based robust force control system with respect to C_F when $m = 0.025$, $K_{Fn} = K_F = 0.675$, $\delta = 1$ and $D_{env} = 1.25$.

different control parameters and environmental impedance in Figs. 7, 8 and 9. As the control gain C_F is increased, the closed-loop discrete poles of the robust force controller move from the open-loop discrete poles indicated by 'x' to the open-loop discrete zeros indicated by 'o'. The unit circle represents the stability region of the discrete controller. In other words, the robust force control system is stable when all of the closed-loop discrete poles are inside the unit circle.

First, it is assumed that the servo system physically interacts with a relatively soft environment ($K_{env} = 275\,N/m$), and the robust force controller is synthesised by using the phase-lag compensators in the inner- and outer- loop (i.e., $\alpha < 1$ and $g_{DOb} > g_{RFOb}$) and the exact values of mass and force coefficient in the RFOb synthesis (i.e., $\delta = 1$). Fig. 7a shows that the robust force controller has underdamped poles for a small value of C_F, and the closed-loop poles move outside the unit circle as the force control gain increases. In other words, oscillatory stable response can be achieved for a limited force control bandwidth. Fig. 7b shows that the stability of the robust force control system can be improved by using the phase-lead compensators in the inner- and outer- loop (i.e., $\alpha > 1$ and $g_{DOb} < g_{RFOb}$). However, not only the control parameters but also the environmental impedance changes the stability of the robust force control system. For example, as the stiffness of the environment (K_{env}) increases, the stability deteriorates even if the phase-lead compensators are employed in the robust force controller synthesis (see Fig. 7c). The stability of contact motion with a stiff environment can be improved by increasing the sampling frequency and the bandwidths of the DOb and RFOb as shown in Fig. 7d. However, this generally increases cost because of higher computing power and more precise measurement system requirements in the implementation of the robust force controller.

So far, the exact mass and force coefficient values are used in the RFOb synthesis (i.e., $\delta = 1$). Since the relative degree of the open-loop transfer function is one when $\delta = 1$, a closed-loop pole moves towards the zero at infinity and the stability of the robust force control system deteriorates as C_F increases (see Fig. 7). When the RFOb is synthesised using $\delta \neq 1$, the relative degree of the open-loop transfer function becomes zero and the closed-loop poles converge to finite values (i.e., to the open-loop zeros) as C_F increases (see Fig. 8) The stability of the robust force control system, however, significantly changes by the design parameter δ. Fig. 8a shows that the stability of contact motion with

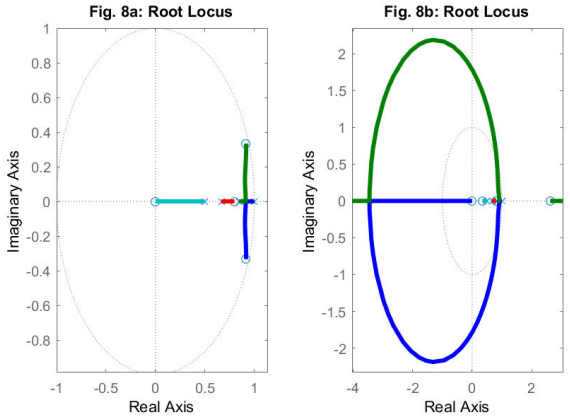

a) $\alpha = 5$ and $\delta = 0.1$ (i.e., $\beta = 50$); b) $\alpha = 5$ and $\delta = 1.1$ (i.e., $\beta = 4.5$).

FIGURE 8. Root-loci of the acceleration-based robust force control system with respect to C_F when $m = 0.025$, $K_{Fn} = K_F = 0.675$, $g_{DOb} = 250$, $g_{RFOb} = 500$, $K_{env} = 2750$, $D_{env} = 1.25$ and $T_s = 1 \times 10^{-3}$.

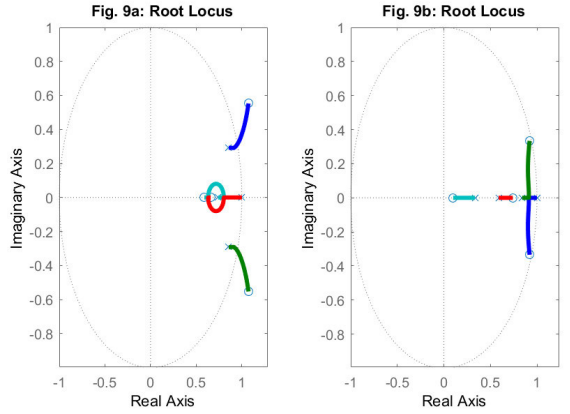

a) $\alpha = 0.2$, $\delta = 1$, $g_{DOb} = 700$ and $g_{RFOb} = 350$, b) $\alpha = 2$, $\delta = 0.1$, $g_{DOb} = 350$ and $g_{RFOb} = 700$.

FIGURE 9. Root-loci of the conventional robust force control system with respect to C_F when $m = 0.025$, $K_{Fn} = K_F = 0.675$, $K_{env} = 2750$, $D_{env} = 1.25$ and $T_s = 1 \times 10^{-3}$.

a stiff environment can be improved without requiring high sampling rate and large bandwidths of the DOb and RFOb when the robust force controller is tuned by using $\delta < 1$. However, Fig. 8b shows that the stability deteriorates by the non-minimum phase zero when $\delta > 1$.

The root-loci of the conventional DOb-based robust force control system are illustrated in Fig. 9. The stabilities of both conventional and acceleration-based robust force control systems have some identical characteristics. For example, while the phase-lag compensators similarly degrade the stability of the robust force control systems as shown in Figs. 7a and 9a, setting the control parameter δ smaller than 1 improves the stability as shown in Figs. 8a and 9b. However, the design constraints of the conventional DOb-based robust force controller are stricter than that of the acceleration-based robust force controller. For example, Fig. 9a shows that the robust force control system has non-minimum phase zeros even if the control parameter δ is equal to 1.

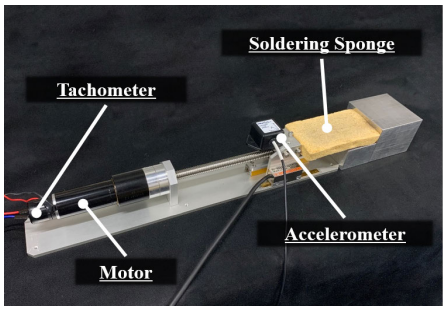

FIGURE 10. Experimental setup.

B. EXPERIMENTS

Force control experiments were performed by using the servo system illustrated in Fig. 10. The experimental setup was built by using Maxon RE25 DC motor, ESCON 50/5 motor driver, DCT22 tachometer to measure the speed of the motor shaft, and Memsic CXL04GP3 accelerometer to measure the acceleration of the linear guide. A PC with a Linux operating system and 2 kHz sampling rate were employed to perform the real-time motion control experiments. Kyowa's LUR-A-200NSA1 load cell was used in the performance evaluation of force control. The mass and force coefficient of the servo system were 0.6kg and 25.1 N/A, respectively, and the lead of the ball screw was 2mm in the experiments.

Let us start with presenting the performance limitation of traditional force control systems. Fig. 11a illustrates the force control experiment of the traditional force controller which is implemented using a simple Proportional (P) controller. It is clear from this figure that the traditional force controller can provide very limited performance due to various disturbances, such as friction and backlash of drivetrain, exerting on the servo system in practice. The force control performance can be significantly improved by employing either the conventional or the acceleration-based robust force controller as illustrated in Figs. 11b and 11c.

Before presenting how the design parameters of the observers change the dynamic response of the DOb-based robust force controllers, let us first verify the performance of the proposed acceleration-based robust force control system illustrated in Fig. 3. Kyowa's load cell was similarly attached to the servo system as recommended in [35] to verify the accuracy of the RFOb. Fig. 12 illustrates the force regulation and trajectory tracking control experiments. When the exact mass and force coefficient values were used in the RFOb synthesis (i.e., $\delta = 1$), external forces were accurately estimated as illustrated in Figs. 12a, 12c and 12e. This is consistent with the general design approach recommended in [9], [12]–[22], [33]. Figs. 12b and 12d show that although the exact mass and force coefficient values were not used in the robust force controller synthesis (i.e., $\delta \neq 1$), the RFOb accurately estimated external forces. However, the accuracy of force estimation deteriorated as the frequency of external force increased as shown in Fig. 12f. This is expected because the effect of the RFOb's design parameters on the

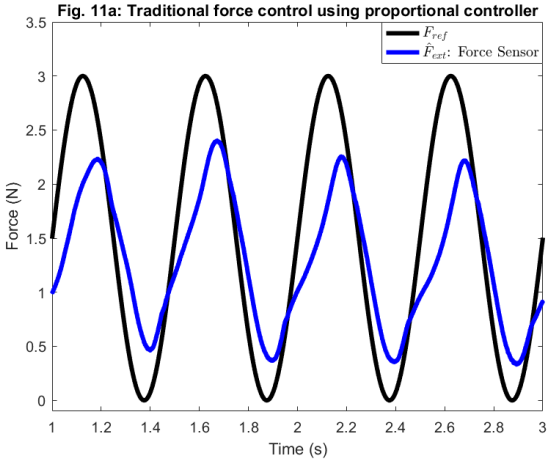

a) Traditional force control implemented by a P-controller.

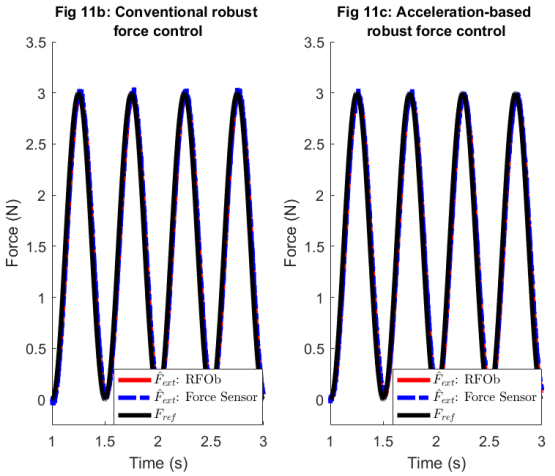

b) Conventional robust force control c) Acceleration-based robust force control

FIGURE 11. 2Hz force trajectory tracking control experiment when the force controllers are synthesised using $C_F = 1$, $g_{DOb} = 200$, $g_{RFOb} = 400$, $\alpha = 2$, $\delta = 1$, and $T_s = 0.5 \times 10^{-3}$.

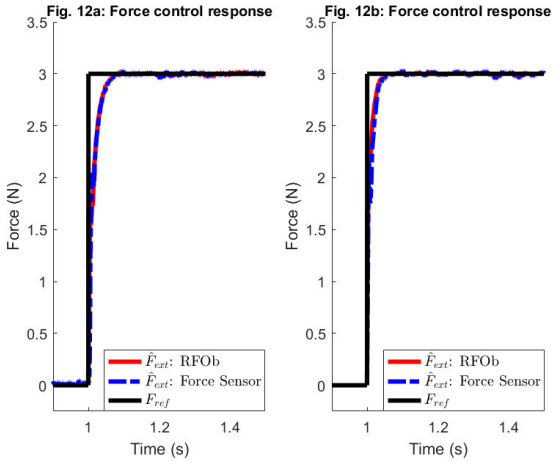

Force regulation control experiment. a) $\delta = 1$, b) $\delta = 0.4$.

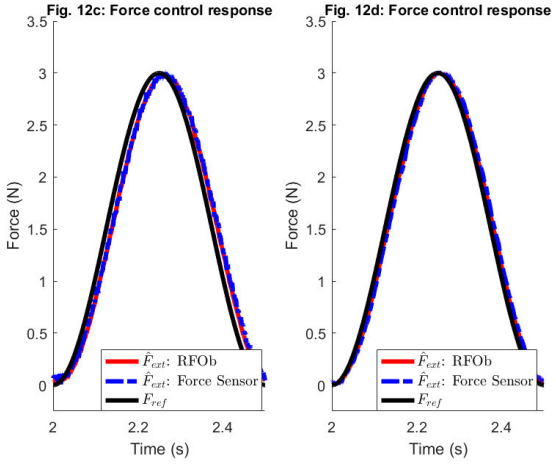

2Hz force trajectory tracking control experiment. c) $\delta = 1$, d) $\delta = 0.4$.

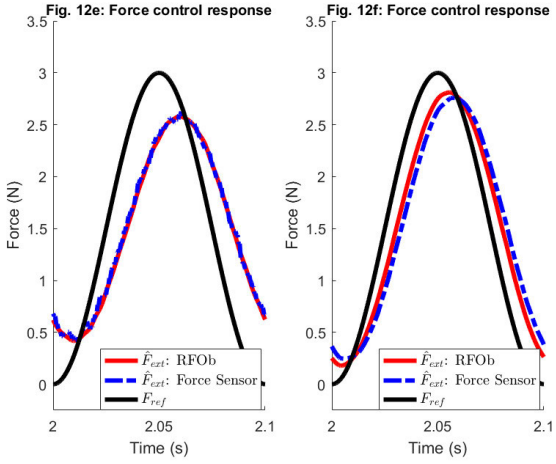

10Hz force trajectory tracking control experiment. e) $\delta = 1$, f) $\delta = 0.4$.

FIGURE 12. Force control experiments when the acceleration-based robust force controller is synthesised using $g_{DOb} = 200$, $g_{RFOb} = 400$, $\alpha = 2$, $C_F = 1$ and $T_s = 0.5 \times 10^{-3}$.

accuracy of force estimation becomes more dominant when the external forces change faster. Compared to the general design approach, Fig. 12 shows that we can tune the mass and force coefficient terms of the RFOb to adjust the stability and performance of the robust force controller while achieving accurate force estimation.

Let us now consider the stability of the DOb-based robust force control systems. Fig. 13 illustrates the force regulation control experiments when different values of nominal mass (i.e., different values of α and β) were used in the robust force controller synthesis. Figs. 13a and 13b show that the robust force controller became unstable when the design constraint of the conventional DOb given in Section II was violated (i.e., $\alpha g_{DOb} > 2\omega_s$). The acceleration-based robust force controller was, however, stable for all values of the design parameter α as shown in Figs. 13c and 13d. Therefore, higher phase-margins can be obtained in the inner-loop when the DOb is implemented using acceleration measurement. Although there is no stability constraint on the design parameters of the acceleration-based DOb, Fig. 13d shows that higher overshoot and oscillatory force control responses were observed when α was increased. This is expected because Section III shows that the open-loop force control gain $\hat{C}_F$ increases when higher/lower values of nominal mass/force

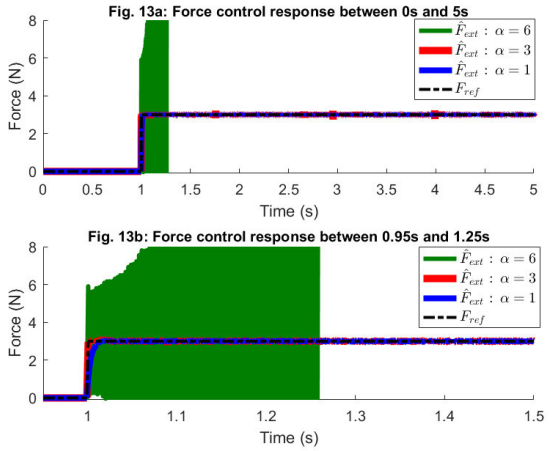

Conventional robust force controller.

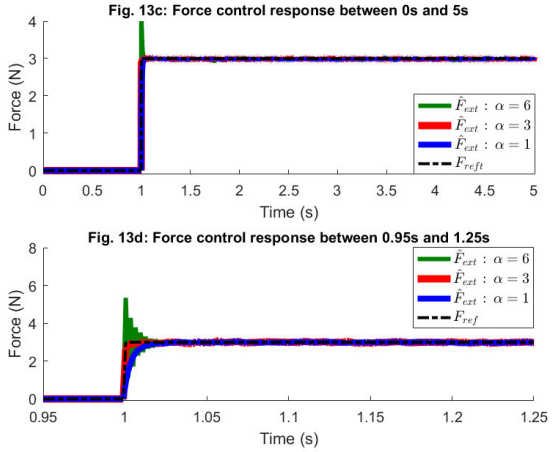

Acceleration-based robust force controller.

FIGURE 13. Force control experiments when the conventional and acceleration-based robust force controllers are synthesised using $g_{DOb} = 500$, $g_{RFOb} = 500$, $\delta = 1$, $C_F = 0.6$, $T_s = 1 \times 10^{-3}$ and the different values of α.

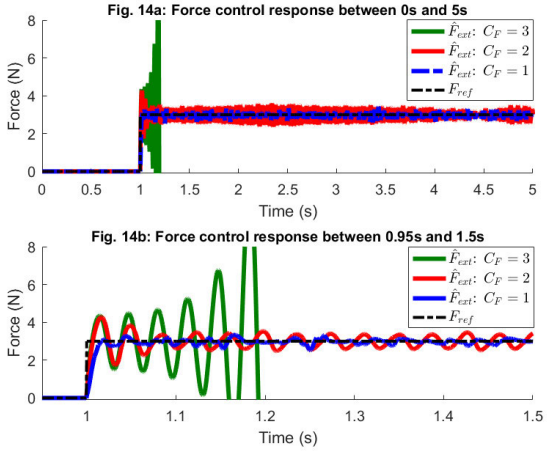

Phase-lag compensators are synthesised using α = 0.5, g_{DOb} = 400 and g_{RFOb} = 200.

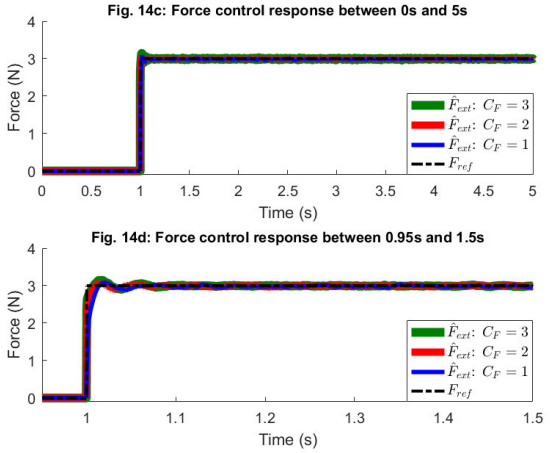

Phase-lead compensators are synthesised using α = 2, g_{DOb} = 200 and g_{RFOb} = 400.

FIGURE 14. Force control experiments when the acceleration-based robust force controller is synthesised using $\delta = 1$, $T_s = 0.5 \times 10^{-3}$ and the phase-lead/lag compensators in the inner- and outer- loop.

coefficient (i.e., higher values of α and β) are used in the robust force controller synthesis. It is clear from this figure that the inner-and outer-loop control parameters should be properly tuned to fulfill high-performance force control tasks.

As shown in Sections II and III, the stability and performance of the robust force controller can be adjusted by tuning the phase-lead/lag compensators in the inner- and outer- loop. This is illustrated in Fig. 14. When the phase-lag compensators were synthesised using $\alpha < 1$ and $g_{DOb} > g_{RFOb}$ in the inner- and outer- loop, respectively, the robust force controller exhibited higher overshoots and oscillatory force control responses as the force control gain C_F was increased (see Figs. 14a and 14b). We could achieve stable contact motion within a limited force control bandwidth, and the robust force controller became unstable when $C_F = 3$. Figs. 14c and 14d show that the stability and force control bandwidth of the robust force controller were improved by using the phase-lead compensators (i.e., $\alpha > 1$ and $g_{DOb} < g_{RFOb}$) in the inner- and outer- loop. Without exhibiting high- overshoots and oscillations, the servo system performed stable contact motion for all values of the force control gain $C_F \leq 3$.

Last, let us show how the design parameter δ influences the stability and performance of the robust force controller. Fig. 15 illustrates the force regulation control experiments when the different values of δ were used in the robust force controller synthesis. To achieve good stability, the acceleration-based robust force controller was synthesised by using the phase-lead compensators in the inner- and outer-loop. Figs. 15a and 15b show that the non-minimum-phase zero had a notable effect on the stability and force control bandwidth of the robust force controller when the RFOb was tuned using $\delta > 1$. Although the phase-lead compensators were employed in the robust force controller synthesis, high-overshoots and oscillations were exhibited when $C_F < 3$. The robust force controller was unstable when $C_F \geq 3$. Figs. 15c and 15d show that using $\delta < 1$ in the RFOb

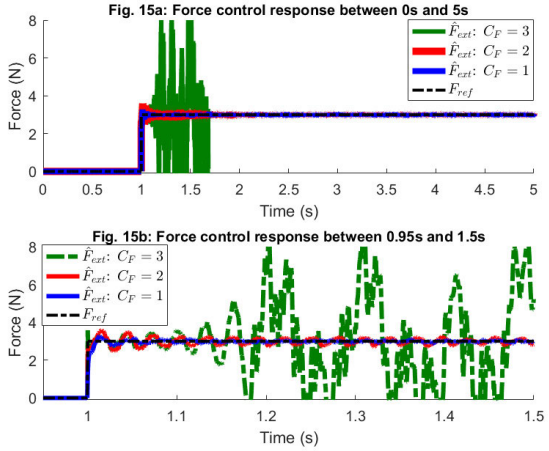

Robust force controller is synthesised using $\delta = 10$.

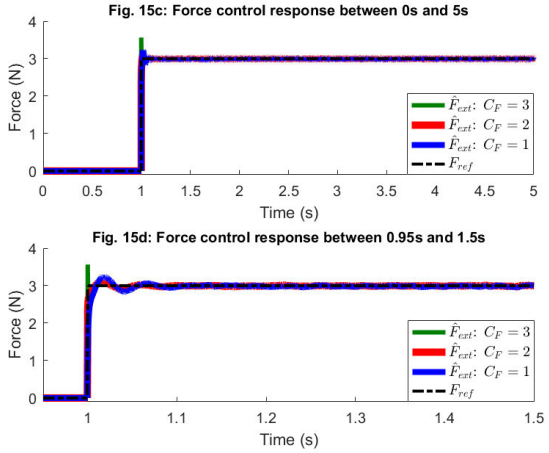

Robust force controller is synthesised using $\delta = 0.1$.

FIGURE 15. Force control experiments when the acceleration-based robust force controller is synthesised using $\alpha = 3$, $g_{DOb} = 200$, $g_{RFOb} = 400$, $T_S = 0.5 \times 10^{-3}$ and the different values of δ.

synthesis significantly improved the stability and force control bandwidth of the robust force controller. Stable contact motion was performed without exhibiting high- overshoots and oscillatory force control responses for all values of the force control gain when $C_F \leq 3$.

C. DISCUSSION ON RESULTS

While traditional force controllers, such as a P-controller, provide limited performance in force control, the DOb-based robust force controller can precisely follow force reference trajectories by suppressing disturbances as shown in Fig. 11. However, the stability and performance of the robust force controller significantly change by the design parameters of the DOb and RFOb. For example, if the identified inertia and force coefficient are not properly tuned, then there is a strict limitation on the bandwidth of force control due to a non-minimum phase zero(s) (see Figs. 8 and 15). Another example is that the stability of the robust controller can be improved by adjusting the phase-lead effect in the inner- and outer- loop via α, g_{DOb} and g_{RFOb} (see Fig. 14). The design parameters of the observers have a notable effect on the stability and performance of the robust force controller. It is, therefore, essential to understand how the dynamic response of the robust force controller changes by the design parameters of the DOb and RFOb.

As shown in Fig. 6, the nominal design parameters and the bandwidth of the conventional DOb are limited not only by noise-sensitivity but also by the waterbed effect. The latter design constraint can be eliminated by employing acceleration measurement in the observer synthesis as shown in Fig. 7. In theory, acceleration-based DOb allows us to improve the robustness against disturbances in the inner-loop and increase the frequency range of contact force estimation in the outer-loop. In practice, the bandwidths of the DOb and RFOb are, however, limited by the noise sensitivity of acceleration measurement systems. This paper presents promising experimental results for the acceleration-based robust force controller in Figs. 12 – 15.

Compared to the conventional design approach, this paper shows that high-performance contact force estimation can still be obtained when the identified mass and force coefficient terms are different than the exact parameters of the servo system (see Figs. 12b, 12d and 12f). This enhances the flexibility in controller synthesis by allowing us to use the identified mass and force coefficient terms as control parameters. For example, Fig. 15 shows that the stability of the robust force controller can be improved by using lower values of the identified mass in the RFOb synthesis.

In addition to the design parameters of the DOb and RFOb, environmental impedance has a notable effect on the stability and performance of the robust force controller. For example, Fig. 7 shows how the stability deteriorates as the stiffness of environment increases. This problem can be tackled by employing an adaptive control algorithm which tunes the design parameters of the robust force controller for changing environmental impedance. For the sake of brevity, adaptive force control is not discussed in this paper. Reader is referred to [5] for an example of the DOb-based adaptive robust force controller.

V. CONCLUSION

The DOb-based robust motion control systems are always implemented using computers and microcontrollers. Yet they are generally analysed and synthesised in the continuous-time domain due to simplicity. Although continuous-time analysis methods are useful to explain the asymptotic behaviours of the DOb (e.g., the higher the bandwidth of the observer, the more the disturbance suppression increases at low frequencies), they fall-short in explaining the robust stability and performance of the digital robust motion control systems. This paper shows that the conventional DOb-based digital robust motion controller is subject to the waterbed effect. Therefore, the stability of the robust motion controller deteriorates as the bandwidth of the conventional DOb increases. To tackle this problem, this paper proposes the acceleration-based DOb.

Conventionally, the exact values of mass and force coefficient are used in the DOb and RFOb synthesis. The bandwidth of the observer is set as high as possible to improve the performance of disturbance and external force estimation. One of the main drawbacks of this design approach is that the exact dynamic model of a motion control system (e.g., the inertia matrix of a robot manipulator) cannot be identified in many engineering applications. It is, therefore, essential to understand how the design parameters of the DOb and RFOb influence the stability and performance of the robust force control systems. For example, the non-minimum phase zero notably deteriorates the stability of the robust force controller when $\delta > 1$ (see Figs. 15a and 15b). Another main drawback is that the conventional design approach does not allow us to adjust the stability and performance of the robust force controller by tuning the design parameters of the DOb and RFOb. However, this paper shows that the stability of the robust force controller can be improved by using higher (lower) values of the mass term in the DOb (RFOb) synthesis (see Figs. 14 and 15).

Although the DOb has been applied to various motion control applications in the last three decades, the control parameters are generally tuned by trial and error. This paper shows that the control parameters of the DOb and RFOb significantly change the stability and performance of the robust force controller. To safely conduct high-performance motion control applications in practice, new design tools that systematically tune the control parameters of the DOb-based digital robust motion control systems should be developed.

REFERENCES

[1] A. Bicchi, M. A. Peshkin, and J. E. Colgate, "Safety for physical human-robot interaction," in *Springer Handbook of Robotics*, 1st ed., B. Siciliano, and O. Khatib Ed. Cham, Switzerland: Springer, 2016, pp. 1335–1348.

[2] A. D. Santis, B. Siciliano, A. De Luca, and A. Bicchi, "An atlas of physical human–robot interaction," *Mech. Mach. Theory*, vol. 43, no. 3, pp. 253–270, Mar. 2008.

[3] M. A. Roa, D. Berenson, and W. Huang, "Mobile manipulation: Toward smart manufacturing [TC spotlight]," *IEEE Robot. Autom. Mag.*, vol. 22, no. 4, pp. 14–15, Dec. 2015.

[4] C. C. Kemp, A. Edsinger, and E. Torres-Jara, "Challenges for robot manipulation in human environments," *IEEE Robot. Autom. Mag.*, vol. 14, no. 1, pp. 20–29, Apr. 2007.

[5] E. Sariyildiz and K. Ohnishi, "An adaptive reaction force observer design," *IEEE/ASME Trans. Mechatronics*, vol. 20, no. 2, pp. 750–760, Apr. 2015.

[6] S. Chen, Z. Chen, B. Yao, X. Zhu, S. Zhu, Q. Wang, and Y. Song, "Adaptive robust cascade force control of 1-DOF hydraulic exoskeleton for human performance augmentation," *IEEE/ASME Trans. Mechatronics*, vol. 22, no. 2, pp. 589–600, Apr. 2017.

[7] Y. Karayiannidis, C. Smith, F. E. V. Barrientos, P. Ögren, and D. Kragic, "An adaptive control approach for opening doors and drawers under uncertainties," *IEEE Trans. Robot.*, vol. 32, no. 1, pp. 161–175, Feb. 2016.

[8] E. Sariyildiz and K. Ohnishi, "On the explicit robust force control via disturbance observer," *IEEE Trans. Ind. Electron.*, vol. 62, no. 3, pp. 1581–1589, Mar. 2015.

[9] S. Kim, S. Choi, H. Kim, J. Shin, H. Shim, and H. J. Kim, "Robust control of an equipment-added multirotor using disturbance observer," *IEEE Trans. Control Syst. Technol.*, vol. 26, no. 4, pp. 1524–1531, Jul. 2018.

[10] B. Ugurlu, M. Nishimura, K. Hyodo, M. Kawanishi, and T. Narikiyo, "Proof of concept for robot-aided upper limb rehabilitation using disturbance observers," *IEEE Trans. Human-Mach. Syst.*, vol. 45, no. 1, pp. 110–118, Feb. 2015.

[11] Y. Wang, H. Fujimoto, and S. Hara, "Driving force distribution and control for EV with four in-wheel motors: A case study of acceleration on split-friction surfaces," *IEEE Trans. Ind. Electron.*, vol. 64, no. 4, pp. 3380–3388, Apr. 2017.

[12] E. Sariyildiz, R. Oboe, and K. Ohnishi, "Disturbance observer-based robust control and its applications: 35th anniversary overview," *IEEE Trans. Ind. Electron.*, vol. 67, no. 3, pp. 2042–2053, Mar. 2020.

[13] K. Ohnishi, S. Katsura, and T. Shimono, "Motion control for real-world haptics," *IEEE Ind. Electron. Mag.*, vol. 4, no. 2, pp. 16–19, Jun. 2010.

[14] A. Suzuki and K. Ohnishi, "Novel four-channel bilateral control design for haptic communication under time delay based on modal space analysis," *IEEE Trans. Control Syst. Technol.*, vol. 21, no. 3, pp. 882–890, May 2013.

[15] S. Katsura, Y. Matsumoto, and K. Ohnishi, "Analysis and experimental validation of force bandwidth for force control," *IEEE Trans. Ind. Electron.*, vol. 53, no. 3, pp. 922–928, Jun. 2006.

[16] H. Kobayashi, S. Katsura, and K. Ohnishi, "An analysis of parameter variations of disturbance observer for motion control," *IEEE Trans. Ind. Electron.*, vol. 54, no. 6, pp. 3413–3421, Dec. 2007.

[17] S. Katsura, K. Irie, and K. Ohishi, "Wideband force control by position-acceleration integrated disturbance observer," *IEEE Trans. Ind. Electron.*, vol. 55, no. 4, pp. 1699–1706, Apr. 2008.

[18] C. Mitsantisuk, K. Ohishi, S. Urushihara, and S. Katsura, "Kalman filter-based disturbance observer and its applications to sensorless force control," *Adv. Robot.*, vol. 25, nos. 3–4, pp. 335–353, Apr. 2011.

[19] T. T. Phuong, K. Ohishi, and Y. Yokokura, "Fine sensorless force control realization based on dither periodic component elimination Kalman filter and wide band disturbance observer," *IEEE Trans. Ind. Electron.*, vol. 67, no. 1, pp. 757–767, Jan. 2020.

[20] E. Sariyildiz, H. Sekiguchi, T. Nozaki, B. Ugurlu, and K. Ohnishi, "A stability analysis for the acceleration-based robust position control of robot manipulators via disturbance observer," *IEEE ASME Trans. Mechatron.*, vol. 23, no. 5, pp. 2369–2378, Oct. 2018.

[21] T. Murakami, N. Oda, Y. Miyasaka, and K. Ohnishi, "A motion control strategy based on equivalent mass matrix in multidegree-of-freedom manipulator," *IEEE Trans. Ind. Electron.*, vol. 42, no. 2, pp. 123–130, Apr. 1995.

[22] E. Sariyildiz, S. Hangai, T. Uzunovic, T. Nozaki, and K. Ohnishi, "Stability and robustness of the disturbance observer-based motion control systems in discrete-time domain," *IEEE/ASME Trans. Mechatronics*, vol. 26, no. 4, pp. 2139–2150, Aug. 2021.

[23] I. Godler, H. Honda, and K. Ohnishi, "Design guidelines for disturbance observer's filter in discrete time," in *Proc. 7th Int. Workshop Adv. Motion Control.*, Maribor, Slovenia, 2002, pp. 390–395.

[24] M. Bertoluzzo, G. S. Buja, and E. Stampacchia, "Performance analysis of a high-bandwidth torque disturbance compensator," *IEEE/ASME Trans. Mechatronics*, vol. 9, no. 4, pp. 653–660, Dec. 2004.

[25] T. Uzunovic, E. Sariyildiz, and A. Sabanovic, "A discussion on discrete implementation of disturbance-observer-based control," in *Proc. IEEE 15th Int. Workshop Adv. Motion Control (AMC)*, Tokyo, Japan, Mar. 2018, pp. 613–618.

[26] A. Tesfaye, H. S. Lee, and M. Tomizuka, "A sensitivity optimization approach to design of a disturbance observer in digital motion control systems," *IEEE/ASME Trans. Mechatronics*, vol. 5, no. 1, pp. 32–38, Mar. 2000.

[27] K. Kong and M. Tomizuka, "Nominal model manipulation for enhancement of stability robustness for disturbance observer-based control systems," *Int. J. Control, Autom. Syst.*, vol. 11, no. 1, pp. 12–20, Feb. 2013.

[28] R. Antonello, K. Ito, and R. Oboe, "Acceleration measurement drift rejection in motion control systems by augmented-state kinematic Kalman filter," *IEEE Trans. Ind. Electron.*, vol. 63, no. 3, pp. 1953–1961, Mar. 2016.

[29] Q. Hou, S. Ding, and X. Yu, "Composite super-twisting sliding mode control design for PMSM speed regulation problem based on a novel disturbance observer," *IEEE Trans. Energy Convers.*, early access, Apr. 6, 2020, doi: 10.1109/TEC.2020.2985054.

[30] D. Tian, R. Xu, E. Sariyildiz, and H. Gao, "An adaptive switching-gain sliding-mode-assisted disturbance observer for high-precision servo control," *IEEE Trans. Ind. Electron.*, early access, Feb. 9, 2021, doi: 10.1109/TIE.2021.3057004.

[31] I. Horowitz, *Synthesis of Feedback Systems*. New York, NY, USA: Academic, 1963.

[32] B. Wu and E. A. Jonckheere, "A simplified approach to Bode's theorem for continuous-time and discrete-time systems," *IEEE Trans. Autom. Control*, vol. 37, no. 11, pp. 1797–1802, Nov. 1992.

[33] E. Sariyildiz and K. Ohnishi, "A guide to design disturbance observer," *J. Dyn. Syst., Meas., Control*, vol. 136, no. 2, pp. 1–10, Mar. 2014.
[34] K. Natori, T. Tsuji, K. Ohnishi, A. Hace, and K. Jezernik, "Time-delay compensation by communication disturbance observer for bilateral teleoperation under time-varying delay," *IEEE Trans. Ind. Electron.*, vol. 57, no. 3, pp. 1050–1062, Mar. 2010.
[35] E. Sariyildiz and K. Ohnishi, "A comparison study for force sensor and reaction force observer based robust force control systems," in *Proc. IEEE 23rd Int. Symp. Ind. Electron. (ISIE)*, Istanbul, Turkey, Jun. 2014, pp. 1156–1161.

EMRE SARIYILDIZ (Senior Member, IEEE) received the Ph.D. degree in integrated design engineering from Keio University, Yokohama, Japan, in 2014, and in control and automation engineering from Istanbul Technical University, Istanbul, Turkey, in 2016. He was a Research Fellow with the Department of Biomedical Engineering, National University of Singapore, Singapore, from 2014 to 2017. Since April 2017, he has been a Lecturer with the School of Mechanical, Materials, Mechatronic, and Biomedical Engineering, University of Wollongong, Wollongong, NSW, Australia. His research interests include robotics, control and automation, mechatronics, and motion control.

SATOSHI HANGAI (Member, IEEE) received the B.E. degree in system design engineering and the M.E. degree in integrated design engineering from Keio University, Yokohama, Japan, in 2018 and 2020, respectively. His research interests include haptics and motion control.

TARIK UZUNOVIC (Senior Member, IEEE) received the B.Eng. and M.Eng. degrees in electrical engineering from the University of Sarajevo, Sarajevo, Bosnia and Herzegovina, in 2008 and 2010, respectively, and the Ph.D. degree in mechatronics from Sabanci University, Istanbul, Turkey, in 2015. He is currently an Associate Professor with the Department of Automatic Control and Electronics, Faculty of Electrical Engineering, University of Sarajevo. His research interests include control theory, motion control, robotics, and mechatronics.

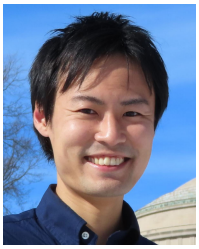

TAKAHIRO NOZAKI (Member, IEEE) received the B.E., M.E., and Ph.D. degrees from Keio University, Yokohama, Japan, in 2010, 2012, and 2014, respectively. In 2014, he joined Yokohama National University, Yokohama, as a Research Associate. In 2015, he joined Keio University, where he is currently an Assistant Professor. He was also a Visiting Scientist with the Massachusetts Institute of Technology, from 2019 to 2021. He was the Winner of the IEEE Industrial Electronics Society Under 35 Innovators Contest, in 2019.